

Theoretical limit of localized surface plasmon resonance sensitivity to local refractive index change and its comparison to conventional surface plasmon resonance sensor

Sergiy J. Zalyubovskiy,^{1,*} Maria Bogdanova,² Alexei Deinega,² Yurii Lozovik,^{2,3} Andrew D. Pris,¹ Kwang Hyup An,¹ W. Paige Hall,¹ and Radislav A. Potyrailo¹

¹GE Global Research Center, 1 Research Circle, Niskayuna, New York 12309, USA

²Kintech Laboratory, Kurchatov Square 1, Moscow 123182, Russia

³Institute for Spectroscopy Russian Academy of Sciences, Fizicheskaya, 5, Troitsk, Moscow region 142190, Russia

*Corresponding author: zalyubov@research.ge.com

Received January 10, 2012; accepted February 23, 2012;
posted March 6, 2012 (Doc. ID 161302); published May 25, 2012

In this paper, the theoretical sensitivity limit of the localized surface plasmon resonance (LSPR) to the surrounding dielectric environment is discussed. The presented theoretical analysis of the LSPR phenomenon is based on perturbation theory. Derived results can be further simplified assuming quasistatic limit. The developed theory shows that LSPR has a detection capability limit independent of the particle shape or arrangement. For a given structure, sensitivity is directly proportional to the resonance wavelength and depends on the fraction of the electromagnetic energy confined within the sensing volume. This fraction is always less than unity; therefore, one should not expect to find an optimized nanofeature geometry with a dramatic increase in sensitivity at a given wavelength. All theoretical results are supported by finite-difference time-domain calculations for gold nanoparticles of different geometries (rings, split rings, paired rings, and ring sandwiches). Numerical sensitivity calculations based on the shift of the extinction peak are in good agreement with values estimated by perturbation theory. Numerical analysis shows that, for thin (≤ 10 nm) analyte layers, sensitivity of the LSPR is comparable with a traditional surface plasmon resonance sensor and LSPR has the potential to be significantly less sensitive to temperature fluctuations. © 2012 Optical Society of America

OCIS codes: 240.6680, 050.6624, 260.3910, 280.4788, 290.3030.

1. INTRODUCTION

Optical properties of noble metal nanoparticles have attracted significant interest in the past decade due to their unique ability to support surface plasmons under optical excitations [1,2]. Surface plasmons are electromagnetic surface waves originating from collective oscillation of conduction electrons near the metal surface. Light coupling into surface plasmons results in enhancement of the local electromagnetic field and strong resonance in the extinction profile called localized surface plasmon resonance (LSPR). The frequency and intensity of LSPR are strongly dependent on nanoparticle shape and composition as well as on surrounding the refractive index, especially in the nanoparticle vicinity [1–4]. The presence of target molecules in the vicinity of the nanoparticle surface can affect the local refractive index. This change can be detected via a shift in LSPR frequency, and hence metal nanoparticles can be utilized as biosensors in various applications [1,5,6].

In thin film surface plasmon resonance (SPR) sensors [3,4], plasmons are generated at the planar interface between metal and dielectric with significant penetration (200–400 nm) of the electromagnetic field into the dielectric medium. Therefore, special techniques should be employed in SPR systems to eliminate influence of the noise in the dielectric bulk. Typical field penetration depth in LSPR geometry is 5–30 nm, which matches well with interrogation volume for biological

monolayers [7,8]. Intrinsically LSPR-based sensors should be less sensitive to bulk noise and require less complex instrumentation. Generally, LSPR has the potential for simplified detection schemes, preserved or improved detection limits, and high-density multiplexing [2,9].

Because of these possibilities, numerous research groups have been investigating various aspects of LSPR systems. Markedly, nearly all of the literature focuses upon discovering a nanofeature geometry that enhances the LSPR sensitivity (e.g., spheres [10–12], rods [13–18], shells [19–25], disks [26–28], rings [29–32], and crescents [33–35]). However, several groups have concentrated on analytical estimation of LSPR sensitivity regardless of nanoparticle geometry. Miller and Lazarides, relying on quasistatic polarizability of particles, showed that bulk sensitivity is proportional to the LSPR wavelength and depends on dispersive properties of the metal [36,37]. Unger and Kreiter found that sensitivity in the quasi-static limit is proportional to the fraction of the electromagnetic energy confined within the volume perturbed by dielectric [38]. The perturbation theory developed by Lai *et al.* [39] for the nonquasistatic case has been adopted by Unger and Kreiter [40] but without taking into account the dispersion characteristic of the metal and without benchmarking LSPR performance against classical SPR sensitivity.

In this paper, we present a study to determine sensitivity limit of LSPR sensors. Obtained results will be used to compare

dependence of the LSPR and SPR sensitivities on the thickness of the analyte layer and to estimate effect of the bulk temperature fluctuations on the signal-to-noise ratio. Theoretical analysis is supported by detailed numerical calculations performed by finite-difference time-domain (FDTD) method [41].

The paper is organized as follows. Section 2 contains derivation of the general LSPR sensitivity expression based on perturbation theory. Simplifications of the sensitivity expression under various assumptions (nondispersive metal, nonabsorbing metal, quasistatic limit) and their applicability to practical sensors are discussed in Section 3. Numerical calculations of the sensitivity for gold nanoparticles of various geometries (rings, split rings, paired rings, and ring sandwiches) are given in Section 4. Comparison between LSPR and SPR sensitivities and signal-to-noise analysis are presented in Section 5. Section 6 summarizes the results.

2. GENERAL PERTURBATION THEORY

The LSPR frequency depends on the shape and dielectric properties $\epsilon_m(\omega)$ of the metal nanoparticle and on the dielectric function of surrounding medium ϵ_d . The dielectric medium is assumed to be lossless and nondispersive $\epsilon_d = n^2$. The sensitivity S is defined as the frequency shift $\Delta\omega$ upon a change in the refractive index Δn :

$$S = \frac{\Delta\omega}{\Delta n}. \quad (1)$$

Refractive index change can occur either in the whole surrounding volume or in the finite layer adjacent to the nanoparticle. These two cases represent bulk and local sensitivity, respectively.

Electric field excitation bound to the surface of the metal particle satisfies wave equation (speed of light $c = 1$ for simplicity)

$$\nabla \times (\nabla \times E_0) - \omega_0^2 \epsilon(\omega_0) E_0 = 0. \quad (2)$$

Note that $\epsilon(\omega_0)$ and therefore resonant frequency ω_0 can be complex variables (imaginary part of ω corresponds to the damping rate). If $\text{Im}(\epsilon_m(\omega_0)) \neq 0$, the problem is non-Hermitian and Eq. (2) is not applicable for complex conjugated field E^* .

Assume that the dielectric function of the surrounding environment has changed by $\Delta\epsilon$. As a consequence, the electric field will have a new configuration $E = E_0 + E_1$, which should satisfy the same wave equation Eq. (2) at a new resonant frequency $\omega = \omega_0 + \Delta\omega$:

$$\begin{aligned} \nabla \times (\nabla \times (E_0 + E_1)) - (\omega_0^2 + 2\omega_0\Delta\omega + \Delta\omega^2) \\ \times \left(\epsilon(\omega_0) + \Delta\epsilon + \left. \frac{\partial\epsilon}{\partial\omega} \right|_{\omega_0} \Delta\omega \right) (E_0 + E_1) = 0. \end{aligned} \quad (3)$$

Terms $\Delta\epsilon$ and $\left. \frac{\partial\epsilon}{\partial\omega} \right|_{\omega_0} \Delta\omega$ have their nonzero values in the dielectric and metal media, respectively: $\Delta\epsilon$ is not zero outside the metal particle due to analyte presence, and $\left. \frac{\partial\epsilon}{\partial\omega} \right|_{\omega_0} \Delta\omega$ is not zero inside the metal because of the resonant frequency shift and dispersion of metal dielectric function. We neglect terms $\left. \frac{\partial^n\epsilon}{\partial\omega^n} \right|_{\omega_0} \Delta\omega^n$, $n > 1$ in expansion for metal dielectric permittivity in Eq. (3).

Neglecting terms of second order of smallness in Eq. (3) and taking into account unperturbed wave equation Eq. (2) results in

$$\begin{aligned} \nabla \times (\nabla \times E_1) - \omega_0^2 \epsilon(\omega_0) E_1 - 2\Delta\omega\omega_0 \epsilon(\omega_0) (E_0 + E_1) \\ - \omega_0^2 \left(\Delta\epsilon + \Delta\omega \left. \frac{\partial\epsilon}{\partial\omega} \right|_{\omega_0} \right) (E_0 + E_1) = 0. \end{aligned} \quad (4)$$

Multiplying Eq. (4) by E_0 [not by E_0^* , since Eq. (2) does not hold for E_0^* if $\text{Im}(\epsilon_m(\omega)) \neq 0$] and integrating over total space V leads to

$$\begin{aligned} \int_V E_0 (\nabla \times (\nabla \times E_1) - \omega_0^2 \epsilon(\omega_0) E_1) dV \\ = 2\Delta\omega\omega_0 \int_V E_0 \epsilon(\omega_0) (E_0 + E_1) dV \\ + \omega_0^2 \int_V E_0 \left(\Delta\epsilon + \Delta\omega \left. \frac{\partial\epsilon}{\partial\omega} \right|_{\omega_0} \right) (E_0 + E_1) dV. \end{aligned} \quad (5)$$

Integrating Eq. (5) twice by parts and using initial Eq. (2) for E_0 results in

$$\begin{aligned} - \oint dS \left(E_0^i \frac{\partial E_1^i}{\partial r} - \frac{\partial E_0^i}{\partial r} E_1^i \right) = 2\Delta\omega\omega_0 \int_V E_0 \epsilon(\omega_0) (E_0 + E_1) dV \\ + \omega_0^2 \int_V E_0 \left(\Delta\epsilon + \Delta\omega \left. \frac{\partial\epsilon}{\partial\omega} \right|_{\omega_0} \right) (E_0 + E_1) dV \\ \times (E_0 + E_1) dV, \end{aligned} \quad (6)$$

where at the first term summation over space indices i is assumed.

The non-Hermitian character of the problem leads to a non-zero surface integral in Eq. (6), which can be evaluated in the far zone. We assume that $\epsilon(\mathbf{r}) \rightarrow 1$ at infinity (otherwise the argumentation can be easily modified); therefore, $k = \omega$ there (since we put speed of light $c = 1$). Taking into account that

$$\begin{aligned} \frac{\partial E^i}{\partial r} \sim \frac{\partial (e^{i\omega r}/r)}{\partial r} = i\omega (e^{i\omega r}/r) \sim i\omega E^i, \\ \frac{\partial E^i}{\partial r} = \frac{\partial (E_0^i + E_1^i)}{\partial r} - \frac{\partial E_0^i}{\partial r} \sim i\omega_0 E_1^i + i\Delta\omega E_0^i, \end{aligned}$$

and neglecting second-order term $\Delta\omega E_1^i$, the surface integral in Eq. (6) can be rewritten as

$$\oint dS \left(E_0^i \frac{\partial E_1^i}{\partial r} - \frac{\partial E_0^i}{\partial r} E_1^i \right) = i\Delta\omega \oint E_0^i E_0^i dS. \quad (7)$$

As a result Eq. (6) turns into

$$\begin{aligned} -i\Delta\omega \oint E_0^2 dS = 2\Delta\omega\omega_0 \int_V E_0 \epsilon(\omega_0) (E_0 + E_1) dV \\ + \omega_0^2 \int_V E_0 \left(\Delta\epsilon + \Delta\omega \left. \frac{\partial\epsilon}{\partial\omega} \right|_{\omega_0} \right) (E_0 + E_1) dV. \end{aligned} \quad (8)$$

Neglecting second-order terms $\Delta\omega E_1$ and $\Delta\epsilon E_1$ leads to

$$-\omega_0^2 \int_V \mathbf{E}_0 \Delta \epsilon \mathbf{E}_0 dV = \Delta \omega \left(\omega_0 \int_V \mathbf{E}_0 \epsilon(\omega_0) \mathbf{E}_0 dV - \omega_0 \int_V \mathbf{E}_0 \frac{\partial(\omega\epsilon)}{\partial\omega} \Big|_{\omega_0} \mathbf{E}_0 dV - i \oint \mathbf{E}_0^2 dS \right). \quad (9)$$

Then frequency shift $\Delta\omega$ can be related to the initial solution E_0 and perturbation $\Delta\epsilon$ as

$$\frac{\Delta\omega}{\omega_0} = \frac{- \int_V \Delta\epsilon \mathbf{E}_0^2 dV}{\int_V \left(\epsilon(\omega_0) + \frac{\partial(\omega\epsilon)}{\partial\omega} \Big|_{\omega_0} \right) \mathbf{E}_0^2 dV + \frac{i}{\omega_0} \oint \mathbf{E}_0^2 dS}. \quad (10)$$

The sensitivity expression $S = \Delta\omega/\Delta n$ can be found by substituting $\Delta\epsilon$ with $2\epsilon(\Delta n/n)$:

$$S = -2 \frac{\omega_0}{n} \frac{\int_{V_d} \epsilon \mathbf{E}_0^2 dV}{\int_V \left(\epsilon(\omega_0) + \frac{\partial(\omega\epsilon)}{\partial\omega} \Big|_{\omega_0} \right) \mathbf{E}_0^2 dV + \frac{i}{\omega_0} \oint \mathbf{E}_0^2 dS}, \quad (11)$$

where V_d and V are volume perturbed by $\Delta\epsilon$ and total system volume, respectively. The surface integral in the denominator of Eq. (11) should be evaluated in the far zone. Multiplying both numerator and denominator of Eq. (11) by the integral over dielectric volume $\int_{V_d} \epsilon \mathbf{E}_0^2 dV$ leads to

$$S = -2 \frac{\omega_0 \tilde{f}}{n} \frac{\int_{V_d} \epsilon \mathbf{E}_0^2 dV}{\int_V \left(\epsilon(\omega_0) + \frac{\partial(\omega\epsilon)}{\partial\omega} \Big|_{\omega_0} \right) \mathbf{E}_0^2 dV + \frac{i}{\omega_0} \oint \mathbf{E}_0^2 dS}, \quad (12)$$

where

$$\tilde{f} = \frac{\int_{V_d} \epsilon \mathbf{E}_0^2 dV}{\int_{V_d} \epsilon \mathbf{E}_0^2 dV}. \quad (13)$$

Equation (12) defines complex quantity S . \mathbf{E}_0^2 denotes scalar product $\mathbf{E} \bullet \mathbf{E}$, not complex conjugation $\mathbf{E}\mathbf{E}^*$. Real part $\text{Re}(S)$ has meaning of the resonance peak shift due to Δn , while imaginary part $\text{Im}(S)$ is related to the change in peak broadening.

3. QUASISTATIC LIMIT

General sensitivity Eq. (12) can be significantly simplified under additional assumptions.

If the metal dielectric function has negligible dispersion in the vicinity of the resonance ω_0 , i.e., $\partial\epsilon/\partial\omega \ll \epsilon$, Eq. (12) reduces to one given by Lai *et al.* [39] (note that the authors of this work took into account the possible degeneracy of unperturbed modes and presented a more complex expression):

$$S = -2 \frac{\omega_0 \tilde{f}}{n} \frac{\int_{V_d} \epsilon \mathbf{E}_0^2 dV}{2 \int_V \epsilon(\omega_0) \mathbf{E}_0^2 dV + \frac{i}{\omega_0} \oint \mathbf{E}_0^2 dS}. \quad (14)$$

If metal is lossless at resonant frequency ($\text{Im}(\epsilon_m) = 0$, $\text{Re}(\epsilon_m) < 0$), the problem Eq. (2) becomes Hermitian and perturbation analysis can be repeated using \mathbf{E}_0^* instead of \mathbf{E}_0 . Equation (12) can be rewritten as

$$S = -2 \frac{\omega_0}{n} f \frac{\int_{V_d} \epsilon |\mathbf{E}_0|^2 dV}{\int_V \left(\epsilon(\omega_0) + \frac{\partial(\omega\epsilon)}{\partial\omega} \Big|_{\omega_0} \right) |\mathbf{E}_0|^2 dV}, \quad (15)$$

$$f = \frac{\int_{V_d} \epsilon |\mathbf{E}_0|^2 dV}{\int_{V_d} \epsilon |\mathbf{E}_0|^2 dV}, \quad (16)$$

where f is the ratio of the energy confined in the volume perturbed by analyte to the energy in whole dielectric bulk. While evaluating integrals in Eq. (16), one can recognize that $V_d \subset V$ and therefore f is always not more than unity. Note that energy is not dissipated in the lossless system and Eq. (15) does not contain a surface integral term.

Interaction of the incident electromagnetic wave with the metal particle can be considered quasistatic if the size of the particle is much smaller than the resonant wavelength. Then the problem is reduced to that of a metal particle in constant external field. This case is the most relevant to biosensing applications since the typical size of the fabricated nanoparticles is 10–100 nm, which is much smaller than the wavelength of the visible or near-infrared light.

In the quasistatic limit, the following expressions can be derived for any local (resonant) mode [42]:

$$\int_V \epsilon(\omega_0) |\mathbf{E}_0|^2 dV = 0 \quad (17)$$

or

$$\int_{V_d} \epsilon(\omega_0) |\mathbf{E}_0|^2 dV = - \int_{V_m} \epsilon(\omega_0) |\mathbf{E}_0|^2 dV. \quad (18)$$

In Eq. (18), first and second integrals are taken over the surrounding dielectric bulk and metal nanoparticle, correspondingly. Substitution of Eq. (18) into Eq. (15) leads to

$$S_{QS} = - \frac{\omega_0}{n} f \frac{2 \int_{V_d} \epsilon |\mathbf{E}_0|^2 dV}{\int_{V_d} \epsilon |\mathbf{E}_0|^2 dV + \int_{V_m} \frac{\partial(\omega\epsilon)}{\partial\omega} \Big|_{\omega_0} |\mathbf{E}_0|^2 dV}. \quad (19)$$

The ratio of the energies stored in metal and dielectric can be expressed as

$$q = \frac{\int_{V_m} \left(\frac{\partial \omega \epsilon}{\partial \omega} \right) |E_0|^2 dV}{\int_{V_d} \epsilon |E_0|^2 dV} = \frac{\int_{V_m} \left(\frac{\partial \omega \epsilon}{\partial \omega} \right) |E_0|^2 dV}{-\int_{V_m} \epsilon |E_0|^2 dV} = -\frac{\frac{\partial (\omega \epsilon_m)}{\partial \omega}}{\epsilon_m}. \quad (20)$$

Combining Eqs. (19) and (20), one can arrive to the following expression for LSPR sensitivity in the quasistatic limit:

$$S_{QS} = -\frac{\omega_0}{n} f \frac{2}{1+q}, \quad (21)$$

$$S_{QS}^i = \frac{\Delta \lambda_0}{\Delta n} = \frac{\lambda_0}{n} f \frac{2}{1+q}. \quad (22)$$

This expression is derived under the assumption that $\text{Im}(\epsilon_m) = 0$. It is also applicable if $|\text{Im}(\epsilon_m)| \ll |\text{Re}(\epsilon_m)|$ in the vicinity of the LSPR frequency. This assumption is valid for gold or silver commonly used to manufacture nanoparticles: for $\lambda_0 = 700$ nm, $|\text{Im}(\epsilon_m)| \sim 1.3$ and $|\text{Re}(\epsilon_m)| \sim 20$. To calculate q , only real part $\text{Re}(\epsilon_m)$ should be used in Eq. (20).

The upper limit for the LSPR sensitivity can be established considering the bounds for f and q . The maximum value of the fill factor f is unity, and it corresponds to the refractive index change in the whole dielectric volume:

$$S_{QS}^i \leq \frac{\lambda_0}{n} \frac{2}{1+q}. \quad (23)$$

If the LSPR wavelength lies in the visible or near-infrared range away from absorption peaks, the q ratio is larger than unity [42]. For noble metals, $\text{Re}(\epsilon(\omega))$ can be approximated well by Drude expression $\epsilon = \epsilon_0 - \omega_p^2/\omega^2$. Typically $\omega_p \gg \omega$, and one can show that

$$q = \frac{\omega_p^2 + \epsilon_0 \omega^2}{\omega_p^2 - \epsilon_0 \omega^2} \approx 1 + 2\epsilon_0 \frac{\omega^2}{\omega_p^2} > 1. \quad (24)$$

Taking into account the above-outlined bounds for $q (> 1)$ and $f (\leq 1)$, the sensitivity of the LSPR has the following upper limit:

$$S_{QS}^i < \frac{\lambda_0}{n}. \quad (25)$$

Analysis of Eqs. (16)–(25) leads to the following general conclusions: (1) sensitivity linearly increases with the LSPR wavelength; (2) the upper limit of the sensitivity is independent of the particle shape, as the upper value for f is unity and q has unity as the lower bound; (3) selection and, possibly, design of particle material should aim at minimizing energy stored in the metal. Indeed, according to the expression for q in the Drude case, an LSPR sensor made of a metal with high plasma frequency ω_p will have better performance.

4. NUMERICAL RESULTS FOR THE LSPR SENSITIVITY

The FDTD numerical method of solving Maxwell's equations [41] was employed to calculate the sensitivity of the LSPRs for various gold nanostructures. Calculations were done with the

help of free simulation package Electromagnetic Template Library, EMTL [43]. The gold dielectric function ($\epsilon_m = \epsilon'(\omega) + i\epsilon''(\omega)$) was represented in Drude–Lorentz form by fitting experimental data in the visible range [44]. (Note that a more sophisticated critical point model allows to fit gold dielectric permittivity in the visible/near-ultraviolet range [45,46]. Recently, implementation of this model in the FDTD using the auxiliary differential equation technique [47] and the recursive convolution technique [48] was reported).

Geometry of the FDTD simulation is shown in Fig. 1. The calculated space (mesh step 2.5 nm) is surrounded by absorbing a perfectly matched layer (PML) [41]. A PML is complemented with an additional back absorbing layer [49] to reduce numerical reflections. The total field (TF)/scattered field (SF) method [41] is used to generate a test plane-wave impulse impinging on nanoparticle. To reduce staircasing effects caused by FDTD rectangular mesh, subpixel smoothing for dielectric permittivity is used [50]. The total (scattered) field is measured by detectors forming a closed surface surrounding nanoparticle in the TF (SF) region. Absorption (scattering) cross-section spectra are calculated by integrating Poynting vector flux over this surface in the TF (SF) region with normalization by the incident flux.

Extinction cross section is obtained as a sum of absorption and scattering cross sections. The plasmonic resonant wavelength is determined by the maximum in the polynomial fit of the extinction spectra near its maximum. Reference extinction in water ($n = 1.33$) for a given structure is calculated first. Then, the uniform dielectric layer ($n = 1.40$) of finite thickness is applied on the nanoparticle to simulate the analyte layer. The extinction spectrum is recalculated, and the spectral shift of the resonance wavelength is translated into sensitivity $S = \Delta\lambda/\Delta n$.

LSPR sensitivities have been calculated numerically for the geometries presented in Fig. 2.

- Standalone rings.
- Split rings with radial 30° segment removed. The cut is oriented either parallel or perpendicular to the light polarization.
- Ring pairs (two rings arranged in-plane at 30 nm distance). The axis connecting the ring centers is either parallel or perpendicular to the light polarization.
- Ring sandwiches (two rings spaced by either 20 or 50 nm along their axis).

The rationale behind the investigation-listed geometries is twofold. First, it has been shown that the wavelength λ_0 of the ring plasmonic resonance can be tuned by geometry across the visible and near-infrared spectral range [29–32]. Second, a certain degree of field enhancement is expected in split rings and closely spaced rings, and its effect on the LSPR sensitivity can be investigated. Rings, used as blocks for the above-listed structures, are characterized by outer diameter

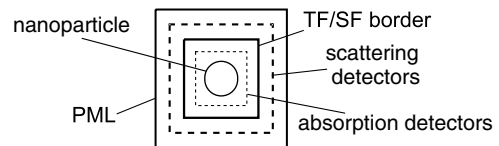


Fig. 1. FDTD simulation three-dimensional cell (cross-sectional view). Scale is not preserved.

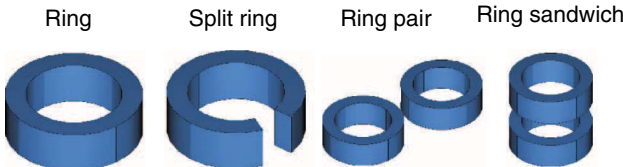


Fig. 2. (Color online) Geometries under consideration.

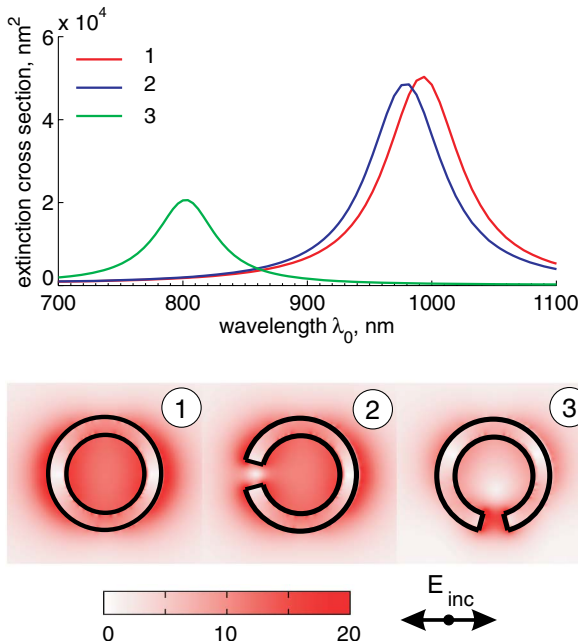
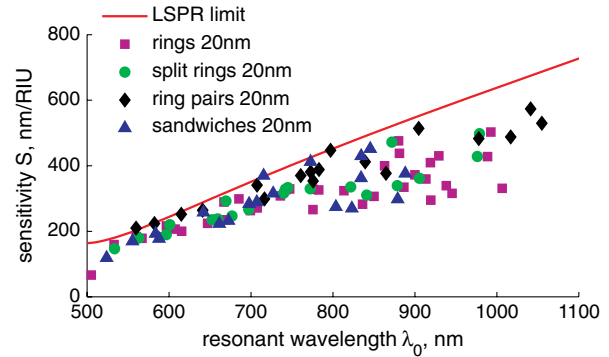
$50 \text{ nm} \leq d \leq 200 \text{ nm}$, height $h \leq 200 \text{ nm}$, width (difference between outer and inner radius) $10 \text{ nm} \leq w \leq 50 \text{ nm}$.

As an illustration, the calculated extinction cross-section spectra and the near-field distributions $|E|/|E_{\text{inc}}|$ at the resonance wavelength for ring and split rings of two cut orientations are presented in Fig. 3. Ring parameters are $d = 75 \text{ nm}$, $w = 10 \text{ nm}$, $h = 20 \text{ nm}$.

The results of the sensitivity calculations for the 20 nm analyte layer are presented in Fig. 4 along with the analytical sensitivity limit S_{QS}^{λ} given by Eq. (22). It should be stressed that, in Eq. (22), fill factor f is taken as unity and gold material properties are used to calculate q . One can see that sensitivity values for various geometries do not exceed theoretical limit S_{QS}^{λ} , thus supporting the earlier statement that upper sensitivity limit does not depend on the geometry of the nanoparticles. As expected, the sensitivity differences are driven mostly by location of the LSPR wavelength in the spectrum.

The theoretical limit is also in agreement with experimentally measured bulk sensitivities for various geometries, as presented in Fig. 5. With exception of two points for nanorods [700 nm/refractive index unit (RIU) at $\lambda_0 = 830 \text{ nm}$ measured by Yu and Irudayaraj [18] and 850 nm/RIU at $\lambda_0 = 1100 \text{ nm}$ measured by Lyvers *et al.* [16]], the experimental sensitivities are close to or below the theoretical limit.

However, Fig. 4 shows that there are geometries, even within the same structural type, with nearly identical LSPR

Fig. 3. (Color online) Extinction cross-section spectra and near-field distributions $|E|/|E_{\text{inc}}|$ (far from a nanoparticle $|E|/|E_{\text{inc}}| = 1$) at the resonance wavelength for ring and split rings of two cut orientations (outer diameter $d = 75 \text{ nm}$, width $w = 10 \text{ nm}$, height $h = 20 \text{ nm}$).Fig. 4. (Color online) Calculated LSPR sensitivities for gold nanoparticles in water as a function of the resonance wavelength λ_0 . Analyte layer -20 nm . Solid line, Eq. (22). Dots of the same shape represent same geometry with different dimensions.

wavelengths but yet varying in sensitivity by as much as 50%. To explain this observation, sensitivities and fill factors were calculated according to Eqs. (12) and (13) for selected geometries. Initially, FDTD simulations were performed for a nanoparticle in unperturbed bulk using extended mesh to ensure that almost all of the SF is confined inside the computational cell. Then, during FDTD simulation, fields E_0 outside and inside of the nanoparticle were recorded at known resonance wavelength using discrete Fourier transformation on the fly. Further integration of the E_0 according to Eq. (12) and (13) results in sensitivity S_{pt} and filling factor \tilde{f} for a given geometry and analyte thickness [note that, for our FDTD set-up, the surface integral was typically less than 2% of volume integrals at Eqs. (12) and (13)]. $\text{Re}(S_{pt})$ and $\text{Re}(\tilde{f})$ along with sensitivity S calculated using shift in extinction spectra are given in Table 2. Typically, $\text{Im}(S_{pt})$ and $\text{Im}(\tilde{f})$ are less than 1% of the real part and therefore neglected. Generally, S_{pt} and S agree qualitatively, and the difference can be explained by the argument that the SF may not necessarily coincide with the plasmon eigenmode on the nanoparticle.

Analysis of the data presented in Table 2 shows that fill factor \tilde{f} plays significant role in defining sensitivity of the nanostructure. Indeed, normalized sensitivities S_{pt}/\tilde{f} shown in Fig. 6 almost coincide with theoretical LSPR limit S_{QS}^{λ} . As an example, one can examine closely the data before and after normalization for the geometries highlighted in Table 2. Highlighted structures have similar λ_0 while sensitivities are significantly different, and after normalization the scatter is removed. Data presented in Fig. 6 and Table 2 also show that

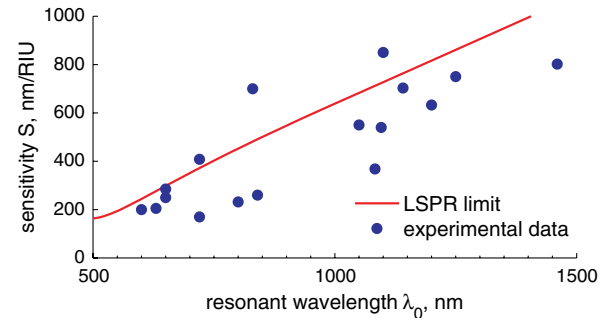


Fig. 5. (Color online) Experimental bulk sensitivities for various geometries as a function of the resonance wavelength. Table 1 provides numerical values, geometrical details, and corresponding references. Solid line, Eq. (22).

Table 1. Experimentally Measured Resonance Wavelengths λ_0 (in nm) and Sensitivities S (in nm/RIU)

Geometry	λ_0	S	Geometry	λ_0	S
Prism [51]	630	205	Disk [28]	1200	633
Rattles [52]	650	285	Shell [25]	720	408
Pyramids [53]	600	200	Star [54]	800	232
Rice [19]	1460	802	Tube [55]	650	250
Rod [15]	720	170	Branch [17]	1141	703
Rod [16]	1100	850	Crescent [35]	1083	368
Rod [17]	1096	540	Ring [29]	1050	550
Rod [14]	840	260	Shell [29]	1250	750
Rod [18]	830	700			

field penetration depth is of the order of 20 nm. Therefore, limited improvements in sensitivity can be achieved by increasing the thickness of the analyte layer.

The presented numerical analysis is in line with theoretical findings, and both are suggesting the same recipe to improve LSPR sensitivity. Generally, the sensor has to be designed to have a resonance at longer wavelengths, and particle geometry should be optimized to increase electromagnetic energy confinement within the analyte.

5. LSPR VERSUS SPR

The superior performance of SPR sensors stems from extreme sensitivity of the plasmon resonance coupling condition to the properties of the dielectric medium. SPR sensors detect changes in the refractive index of the surrounding medium with sensitivities approaching 1400 nm/RIU [56,57]. This sensitivity is achieved in part due to the long decay length of propagating plasmons (200–400 nm), providing detection abilities well into the bulk environment. However, these long decay lengths and superior sensitivity come at the cost of signal to noise when sensing thin analyte layers. In biological sensing applications, where a monolayer of biomolecules generally creates a dielectric layer of 5–30 nm in thickness, the fraction of the electromagnetic energy stored in the analyte for SPR is far below the maximum value of unity. One way to compensate for the lower fill factors inherent to biomolecule detection would be to decrease the size of the sensing volume. Indeed, this is the case with localized SPR, where the sensing volume typically extends 30 nm from the nanoparticle surface.

The wavelength-dependent SPR sensitivity $S(\lambda_R)$ was calculated for the standard Kretschmann configuration. Water ($n = 1.33$) was taken as the working fluid, and calculations were performed for a 50 nm thick gold film on top of a glass prism ($n = 1.53$). SPR manifests itself as a dip in the reflectance spectrum when p -polarized light is incident on the prism at particular angle. This pair—incidence angle and wavelength corresponding to reflectance minimum—represents a momentum matching condition, which is necessary to excite SPR at the gold-fluid interface. Reflectance spectra were calculated based on classical transfer matrix formalism [58] (note that they could be calculated using the FDTD iterative technique for modeling the periodic structures at oblique incidence [59] as well). For a given wavelength λ_R , the incident angle was scanned to determine angle θ_R for which reflectivity reaches its minimum. Then the angle was fixed at θ_R and the spectra were calculated for a bare gold film as well as for a gold film with a 20 or 10 nm thick analyte layer. The sensitivity was calculated from the shift of the resonance wavelength upon addition of the analyte layer. To determine wavelength-dependent sensitivity $S(\lambda_R)$, the calculations were repeated for $\lambda_R = 580$ –1100 nm. The lower wavelength limit 580 nm is determined by increase in gold absorption.

A comparison of the calculated SPR and LSPR sensitivities for 20 and 10 nm analyte layers is presented in Fig. 7. Clearly, sensitivity of the SPR system is superior to that of LSPR for the 20 nm analyte layer. However, the sensitivity of LSPR appears to coalesce with SPR if thickness of the analyte layer decreases to ~10 nm. Furthermore, calculations with variable analyte thicknesses presented in Fig. 8 show that LSPR does have sensitivities similar to SPR for the relevant to biomolecular sensing analytical volumes. Calculations presented in Fig. 8 provide a measure of the LSPR field penetration depth and show LSPR sensitivity saturation as analyte thickness increases beyond 20 nm.

The above discussion of LSPR versus SPR sensitivities is purposefully devoid of noise considerations. However the key metric for analytical instrumentation is not solely sensitivity but rather the achieved detection limit and signal-to-noise ratio. Specifically, SPR will register fluctuations of the refractive index in the test solution outside of the biomolecular layer due to its large bulk sensitivity and long sensing decay lengths. LSPR will be physically insensitive to this noise outside of its field penetration depth. Examples of these noise

Table 2. Sensitivities S (Shifts in Spectra) and S_{pt} [Field Integration according to Eq. (12)], Fill Factors \tilde{f} [according to Eq. (13)], and Normalized Sensitivities S_{pt}/\tilde{f} for the Subset of Investigated Geometries^a

	Dimensions nm	Resonance λ_0 , nm	Analyte 20 nm				Analyte 10 nm			
			S	S_{pt}	\tilde{f}	S_{pt}/\tilde{f}	S	S_{pt}	\tilde{f}	S_{pt}/\tilde{f}
Ring	75/10/20	993	503	424	0.73	583	351	282	0.48	583
	100-10-200	813	324	277	0.64	435	211	191	0.44	435
Split Ring	75/10/20	979	498	449	0.74	607	357	308	0.51	607
	150-50-20	878	339	296	0.54	549	219	187	0.34	550
Sandwich	75/10/20	924	441	369	0.71	523	305	224	0.47	523
Spacing 20 nm	75/10/100	846	452	375	0.82	457	335	292	0.64	457
	150/50/20	821	294	247	0.51	488	184	152	0.31	490
	125/50/100	773	412	369	0.86	431	360	315	0.73	431
	100/20/200	661	223	157	0.58	273	147	106	0.39	274
	50/20/100	524	119	131	0.74	178	78	84	0.52	160

^aFor S_{pt}, \tilde{f} , and S_{pt}/\tilde{f} , real parts are presented (typically the imaginary part for these values are less than 1% of the real part). Dimensions are given in diameter/width/height format.

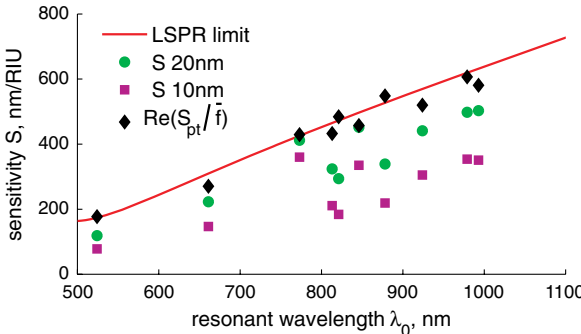


Fig. 6. (Color online) Sensitivities of the nanostructures with and without normalization by filling factor. Geometries and numerical values for λ_0 , S, \bar{f} , and S_{pt}/\bar{f} are provided in Table 2.

contributing fluctuations include heterogeneous bulk distributions of density changes from nonuniform flow profiles, of temperature profiles, and of local concentration of analytes/solutions.

Estimated signal-to-noise (S/N) ratios for sensors based on LSPR and SPR are provided in Fig. 9. Both sensors are probing a 20 nm analyte layer in water. The refractive index of water changes by 10^{-4} RIU per degree K near room temperature [56,60]. Thermal stability ΔT is assumed to be 10 mK, which corresponds to fluctuations $\Delta n_T \sim 10^{-6}$ in bulk refractive index. The change of the refractive index in the analyte layer is taken as $\Delta n_A = 10^{-5}$, which is of the order of SPR sensor resolution [3]. The following equation is used to calculate the S/N ratio for both LSPR and SPR sensors:

$$G_{\text{LSPR,SPR}} = \frac{S}{N} = \frac{\Delta \lambda_S}{\Delta \lambda_N} = \frac{S_{\text{layer}}^{20\text{nm}} \cdot \Delta n_A}{S_{\text{bulk}} \cdot \Delta n_T}, \quad (26)$$

where $S_{\text{layer}}^{20\text{nm}}$ and S_{bulk} are sensitivities to the local and bulk refractive index change, respectively.

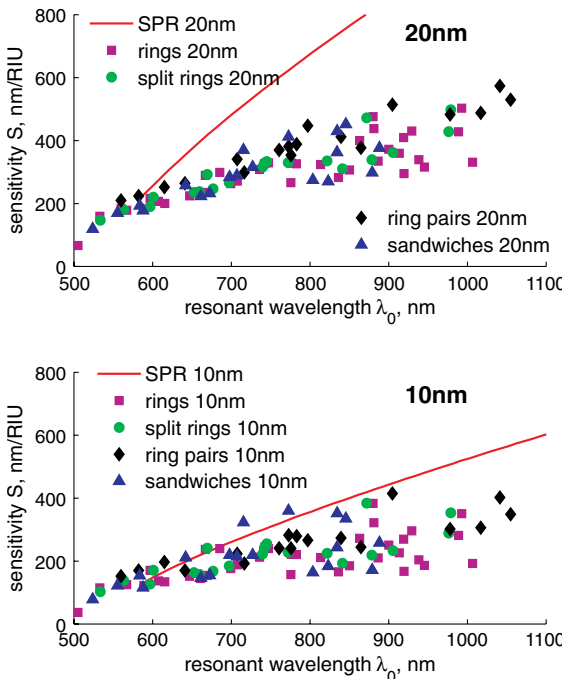


Fig. 7. (Color online) Sensitivity of the LSPR and SPR. Analyte thickness 20 nm (upper) and 10 nm (lower).

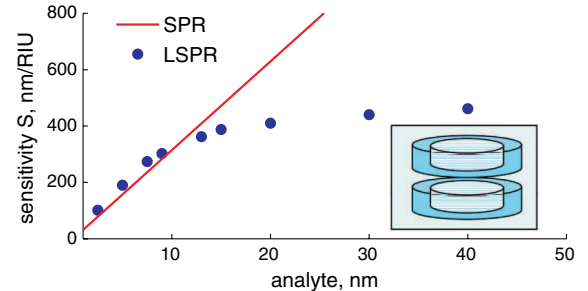


Fig. 8. (Color online) Sensitivity of the LSPR ring sandwich (individual ring geometry, outer diameter $d = 125$ nm, width $w = 100$ nm, height $h = 50$ nm) and SPR as a function of the analyte thickness. Resonance wavelength for both sensors is 770 nm.

As one can see from Fig. 9, LSPR provides a factor of 6–8 improvement in S/N in the case of a thin analyte layer. In fact, one can show that LSPR gain in S/N over SPR does not depend on Δn_T and Δn_A . As evident from Figs. 4 and 8, LSPR bulk sensitivity and sensitivity to the 20 nm analyte layer are close, $S_{\text{layer}}^{20\text{nm}} \approx S_{\text{bulk}}$. Therefore, the LSPR S/N gain over SPR can be written as

$$\frac{G_{\text{LSPR}}}{G_{\text{SPR}}} = \frac{S_{\text{layer}}^{\text{LSPR}}}{S_{\text{bulk}}^{\text{LSPR}}} \cdot \frac{S_{\text{bulk}}^{\text{SPR}}}{S_{\text{layer}}^{\text{SPR}}} \approx \frac{S_{\text{bulk}}^{\text{SPR}}}{S_{\text{layer}}^{\text{SPR}}} \approx 8 \text{ at } 750 \text{ nm.} \quad (27)$$

Estimates also show that 5 mK temperature fluctuations will result in $S/N \approx 3$ for an SPR system sensing a 20 nm analyte layer at 700 nm. The LSPR sensor can tolerate ≈ 30 mK noise to achieve the same S/N ratio for the same analyte layer and resonant frequency.

Commercial SPR systems have multiple engineering and processing solutions to ensure that the noise is muted and an appreciable detection limit is achieved. For example, highly controlled housing is added around the SPR sensor in order to eliminate temperature fluctuations and vibration. This housing performs remarkably well, allowing current state-of-the-art SPR sensors to reach detection limits of 10^{-7} RIU. However, the need for sophisticated instrumentation raises both the cost and the complexity of the SPR system.

This theoretical examination of the S/N characteristics of SPR and LSPR systems has been experimentally vetted by studies comparing biomolecule detection for SPR and LSPR [57,61]. Importantly, in both cases, these separate groups

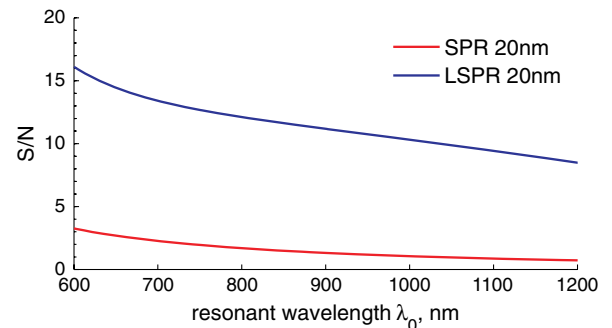


Fig. 9. (Color online) S/N ratio for the LSPR- and SPR-based sensors probing 20 nm analyte layer in water. ΔT is 10 mK, and Δn in the analyte layer is 10^{-5} .

demonstrated similar performance for the two sensor modalities, despite the superior bulk detection ability of SPR.

6. CONCLUSION

Sensitivity of LSPR has a physical limit directly proportional to the resonance wavelength. Given specific resonance wavelength, the sensitivity is governed by fill factor f , defined as the fraction of the electromagnetic energy within the sensing volume. The maximum value of f is unity, and thus the upper limit of the sensitivity does not depend on the shape of the particle. The particle shape and features should be chosen to have LSPR wavelength as far to the infrared as possible in biological assay systems, and fill factor f should be optimized ($f \rightarrow 1$) as well via the geometry of the feature. Particle material should be considered in the design of the LSPR sensor to minimize ($q \rightarrow 1$) energy confined in the metal particle.

Sensitivity of the LSPR is on par with SPR for analyte thickness ≤ 10 nm. Because of the localized nature of plasmonic oscillations excited on the nanoparticles, LSPR is immune to the bulk noise sources that plague SPR systems. LSPR will perform ~ 8 -fold better in terms of S/N as compared to the classic SPR in the same temperature-controlled environment.

ACKNOWLEDGMENTS

This work was supported in part by General Electric Global Research Center Nano Advanced Technology funding and by the Ministry of Science and Education of Russia under the contract no. 16.523.11.3004. Authors graciously thank Margaret Blohm for her support and Tao Deng, Boris Russ, and Wen Shang for technical discussions.

REFERENCES

- K. M. Mayer and J. H. Hafner, "Localized surface plasmon resonance sensors," *Chem. Rev.* **111**, 3828–3857 (2011).
- K. A. Willets and R. P. Van Duyne, "Localized surface plasmon resonance spectroscopy and sensing," *Ann. Rev. Phys. Chem.* **58**, 267–297 (2007).
- J. Homola, S. S. Yee, and Gunter Gauglitz, "Surface plasmon resonance sensors: review," *Sens. Actuators B Chem.* **54**, 3–15 (1999).
- R. B. M. Schasfoort and A. J. Tudos, *Handbook of Surface Plasmon Resonance* (Royal Society of Chemistry, 2008).
- G. J. Nusz, S. M. Marinakos, A. C. Curry, A. Dahlin, F. Hook, A. Wax, and A. Chilkoti, "Label-free plasmonic detection of biomolecular binding by a single gold nanorod," *Anal. Chem.* **80**, 984–989 (2008).
- G. J. Nusz, A. C. Curry, S. M. Marinakos, A. Wax, and A. Chilkoti, "Rational selection of gold nanorod geometry for label-free plasmonic biosensors," *ACS Nano* **3**, 795–806 (2009).
- E. Hao and G. C. Schatz, "Electromagnetic fields around silver nanoparticles and dimers," *J. Chem. Phys.* **120**, 357–366 (2004).
- K. Imura, H. Okamoto, and T. Nagahra, "Plasmon mode imaging of single gold nanorods," *J. Am. Chem. Soc.* **126**, 12730–12731 (2004).
- J. N. Anker, W. P. Hall, O. Lyandres, N. C. Shah, J. Zhao, and R. P. Van Duyne, "Biosensing with plasmonic nanosensors," *Nat. Mater.* **7**, 442–453 (2008).
- N. Nath and A. Chilkoti, "A colorimetric gold nanoparticle sensor to interrogate biomolecular interactions in real time on a surface," *Anal. Chem.* **74**, 504–509 (2002).
- N. Nath and A. Chilkoti, "Label-free biosensing by surface plasmon resonance of nanoparticles on glass: optimization of nanoparticle size," *Anal. Chem.* **76**, 5370–5378 (2004).
- A. J. Haes, S. Zou, G. C. Schatz, and R. P. Van Duyne, "Nanoscale optical biosensor: short range distance dependence of the localized surface plasmon resonance of noble metal nanoparticles," *J. Phys. Chem. B* **108**, 6961–6968 (2004).
- A. L. Schmucker, N. Harris, M. J. Banholzer, M. G. Blaber, K. D. Osberg, G. C. Schatz, and C. A. Mirkin, "Correlating nanorod structure with experimentally measured and theoretically predicted surface plasmon resonance," *ACS Nano* **4**, 5453–5463 (2010).
- G. J. Nusz, A. C. Curry, S. M. Marinakos, A. Wax, and A. Chilkoti, "Rational selection of gold nanorod geometry for label-free plasmonic biosensors," *ACS Nano* **3**, 795–806 (2009).
- K. M. Mayer, S. Lee, H. Liao, B. C. Rostro, A. Fuentes, P. T. Scully, C. L. Nehl, and J. H. Hafner, "A label-free immunoassay based upon localized surface plasmon resonance of gold nanorods," *ACS Nano* **2**, 687–692 (2008).
- D. P. Lyvers, J.-M. Moon, A. V. Kildishev, V. M. Shalaev, and A. Wei, "Gold nanorod arrays as plasmonic cavity resonators," *ACS Nano* **2**, 2569–2576 (2008).
- H. Chen, X. Kou, Z. Yang, W. Ni, and J. Wang, "Shape- and size-dependent refractive index sensitivity of gold nanoparticles," *Langmuir* **24**, 5233–5237 (2008).
- C. Yu and J. Irudayaraj, "Quantitative evaluation of sensitivity and selectivity of multiplex nanoSPR biosensor assays," *Biophys. J.* **93**, 3684–3692 (2007).
- H. Wang, D. W. Brandl, F. Le, P. Nordlander, and N. J. Halas, "Nanorice: a hybrid plasmonic nanostructure," *Nano Lett.* **6**, 827–832 (2006).
- H. Wang, D. W. Brandl, P. Nordlander, and N. J. Halas, "Plasmonic nanostructures: artificial molecules," *Acc. Chem. Res.* **40**, 53–62 (2007).
- E. Prodan, A. Lee, and P. Nordlander, "The effect of a dielectric core and embedding medium on the polarizability of metallic nanoshells," *Chem. Phys. Lett.* **360**, 325–332 (2002).
- E. Prodan and P. Nordlander, "Structural tunability of the plasmon resonances in metallic nanoshells," *Nano Lett.* **3**, 543–547 (2003).
- M. Cao, M. Wang, and N. Gu, "Optimized surface plasmon resonance sensitivity of gold nanoboxes for sensing applications," *J. Phys. Chem. C* **113**, 1217–1221 (2009).
- L. J. Sherry, S.-H. Chang, G. C. Schatz, and R. P. Van Duyne, "Localized surface plasmon resonance spectroscopy of single silver nanocubes," *Nano Lett.* **5**, 2034–2038 (2005).
- Y. Sun and Y. Xia, "Increased sensitivity of surface plasmon resonance of gold nanoshells compared to that of gold solid colloids in response to environmental changes," *Anal. Chem.* **74**, 5297–5305 (2002).
- S. R. Beiram and F. P. Zamborini, "Purification of gold nanoplates grown directly on surfaces for enhanced localized surface plasmon resonance biosensing," *ACS Nano* **4**, 3633–3646 (2010).
- A. Dmitriev, C. Hagglund, Si Chen, H. Fredriksson, T. Pakizeh, M. Kall, and D. S. Sutherland, "Enhanced nanoplasmonic optical sensors with reduced substrate effect," *Nano Lett.* **8**, 3893–3898 (2008).
- Y. Sonnenaud, N. Verellen, H. Sobhani, G. Vandenbosch, V. Moshchalkov, P. Van Dorpe, P. Nordlander, and S. Maier, "Experimental realization of subradiant, superradiant, and Fano resonances in ring/disk plasmonic nanocavities," *ACS Nano* **4**, 1664–1670 (2010).
- E. M. Larsson, J. Alegret, M. Kall, and D. S. Sutherland, "Sensing characteristics of NIR localized surface plasmon resonances in gold nanorings for application as ultrasensitive biosensors," *Nano Lett.* **7**, 1256–1263 (2007).
- F. Hao, P. Nordlander, Y. Sonnenaud, P. Van Dorpe, and S. A. Maier, "Tunability of subradiant dipolar and Fano-type plasmon resonances in metallic ring/disk cavities: implications for nanoscale optical sensing," *ACS Nano* **3**, 643–652 (2009).
- J. Aizpurua, P. Hanarp, D. S. Sutherland, M. Kall, G. W. Bryant, and F. J. García de Abajo, "Optical properties of gold nanorings," *Phys. Rev. Lett.* **90**, 057401 (2003).
- C. M. Dutta, T. A. Ali, D. W. Brandl, T.-H. Park, and P. Nordlander, "Plasmonic properties of a metallic torus," *J. Chem. Phys.* **129**, 084706 (2008).
- A. K. Sheridan, A. W. Clark, A. Glidle, J. M. Cooper, and D. R. S. Cumming, "Multiple plasmon resonances from gold nanostructures," *Appl. Phys. Lett.* **90**, 143105 (2007).
- F. Hao, Y. Sonnenaud, P. Van Dorpe, S. A. Maier, N. J. Halas, and P. Nordlander, "Symmetry breaking in plasmonic nanocavities:

- subradiant LSPR sensing and a tunable Fano resonance," *Nano Lett.* **8**, 3983–3988 (2008).
35. R. Bukasov and J. S. Shumaker-Parry, "Highly tunable infrared extinction properties of gold nanocrescents," *Nano Lett.* **7**, 1113–1118 (2007).
 36. M. M. Miller and A. A. Lazarides, "Sensitivity of metal nanoparticle surface plasmon resonance to the dielectric environment," *J. Phys. Chem. B* **109**, 21556–21565 (2005).
 37. M. M. Miller and A. A. Lazarides, "Sensitivity of metal nanoparticle plasmon resonance band position to the dielectric environment as observed in scattering," *J. Opt. A* **8**, S239–S249 (2006).
 38. A. Unger and M. Kreiter, "Detecting molecules with plasmonic resonators—analytic expressions and bounds for the sensitivity and figure of merit," preprint, <http://arxiv.org/abs/1007.0837>.
 39. H. M. Lai, P. T. Leung, K. Young, P. W. Barber, and S. C. Hill, "Time-independent perturbation for leaking electromagnetic modes in open systems with application to resonances in microdroplets," *Phys. Rev. A*, **41** 5187–5198 (2009).
 40. A. Unger and M. Kreiter, "Analyzing the performance of plasmonic resonators for dielectric sensing," *J. Phys. Chem. C* **113**, 12243–12251 (2009).
 41. A. Tafove and S. H. Hagness, *Computational Electrodynamics: The Finite Difference Time-Domain Method* (Artech, 2005).
 42. F. Wang and Y. R. Shen, "General properties of local plasmons in metal nanostructures," *Phys. Rev. Lett.* **97**, 206806 (2006).
 43. Electromagnetic Template Library, <http://fdtd.kintechlab.com>.
 44. J. M. McMahon, J. Henzie, T. W. Odom, G. C. Schatz, and S. K. Gray, "Tailoring the sensing capabilities of nanohole arrays in gold films with Rayleigh anomaly-surface plasmon polaritons," *Opt. Express* **15**, 18119–18129 (2007).
 45. P. G. Etchegoin, E. C. Le Ru, and M. Meyer, "An analytic model for the optical properties of gold," *J. Chem. Phys.* **125**, 164705 (2006).
 46. <http://fdtd.kintechlab.com/en/fitting>.
 47. A. Deinega and S. John, "Effective optical response of silicon to sunlight in the finite-difference time-domain method," *Opt. Lett.* **37**, 112–114 (2012).
 48. A. Vial, "Implementation of the critical points model in the recursive convolution method for dispersive media modeling with the FDTD methods," *J. Opt. A* **9**, 745–748 (2007).
 49. A. Deinega and I. Valuev, "Long-time behavior of PML absorbing boundaries for layered periodic structures," *Comput. Phys. Commun.* **182**, 149–151 (2011).
 50. A. Deinega and I. Valuev, "Subpixel smoothing for conductive and dispersive media in the FDTD method," *Opt. Lett.* **32**, 3429–3431 (2007).
 51. L. J. Sherry, R. Jin, C. A. Mirkin, G. C. Schatz, and R. P. Van Duyne, "Localized surface plasmon resonance spectroscopy of single silver triangular nanoprisms," *Nano Lett.* **6**, 2060–2065 (2006).
 52. Y. Khalavka, J. Becker, and C. Solonichsen, "Synthesis of rod-shaped gold nanorattles with improved plasmon sensitivity and catalytic activity," *J. Am. Chem. Soc.* **131**, 1871–1875 (2009).
 53. E. A. Coronado and G. C. Schatz, "Surface plasmon broadening for arbitrary shape nanoparticles: a probability approach," *J. Chem. Phys.* **119**, 3926–3934 (2003).
 54. C. Nehl, H. Liao, and J. Hafner, "Optical properties of star-shaped gold nanoparticles," *Nano Lett.* **6**, 683–688 (2006).
 55. J. McPhillips, A. Murphy, M. Jonsson, W. Hendren, R. Atkinson, H. Fredrik, A. Zayats, and R. Pollard, "High-performance biosensing using arrays of plasmonic nanotubes," *ACS Nano* **4**, 2210–2216 (2010).
 56. L. S. Jung, C. T. Campbell, T. M. Chinowsky, M. N. Mar, and S. S. Yee, "Quantitative interpretation of the response of surface plasmon resonance sensors to adsorbed films," *Langmuir* **14**, 5636–5648 (1998).
 57. M. Svedendahl, S. Chen, A. Dmitriev, and M. Kall, "Refractometric sensing using propagating versus localized surface plasmons: a direct comparison," *Nano Lett.* **9**, 4428–4433 (2009).
 58. M. Born and E. Wolf, *Principles of Optics* (Pergamon, 1980).
 59. I. Valuev, A. Deinega, and S. Belousov, "Iterative technique for analysis of periodic structures at oblique incidence in the finite-difference time-domain method," *Opt. Lett.* **33**, 1491–1493 (2008).
 60. D. R. Lide, ed., *Handbook of Chemistry Physics*, 71st ed. (CRC Press, 1990).
 61. C. R. Yonzon, E. Jeoung, S. Zou, G. C. Schatz, M. Mrksich, and R. P. Van Duyne, "A comparative analysis of localized and propagating surface plasmon resonance sensors: the binding of Concanavalin A to a monosaccharide functionalized self-assembled monolayer," *J. Am. Chem. Soc.* **126**, 12669–12676 (2004).